JOURNAL OF MATERIALS SCIENCE **37** (2002) 397–410

Origins of hindrance in densification of Ag/Al_2O_3 composites

K. MAEKAWA, Y. NAKADA, T. KIMURA
Faculty of Science and Technology, Keio University, 3-14-1 Hiyoshi, Kohoku-ku, Yokohama 223-8522 Japan
E-mail: kimura@applc.keio.ac.jp

The densification and microstructure development were studied for Ag-matrix composites containing dispersed Al_2O_3 particles to examine the effect of inclusions on the densification of composites. The incorporation of Al_2O_3 particles into Ag matrix hindered densification. Microstructure observation revealed that pores larger than those in the matrix formed around Al_2O_3 particles during sintering. The pore morphology was dependent on the number density of Al_2O_3 particles. When the number density was low, pores remained around an Al_2O_3 particle and coalesced to a large circumferential void at high temperatures. When the number density was intermediate, clusters made of a few Al_2O_3 particles formed and pores within and around clusters remained up to high temperatures. When the number density was high, the distance between clusters became small and the clusters were connected, forming continuous pores (pore channels). The three-dimensional connectivity of Ag was decreased, and the shrinkage between Ag particles resulted in thickening of pore channels. The presence of these large pores was the origin of the hindrance in densification.

1. Introduction

Composites with dispersed particles are used to improve the mechanical properties of metals, ceramics, and polymers. In metal-matrix composites, the matrix is strengthened and hardened by the uniform dispersion of several volume percent of fine particles of a very hard and inert material. In ceramic-matrix composites, inherent brittleness of ceramics is overcome by incorporation of ceramic whiskers, strong fibers, and particulates. Although dispersed particles improve the mechanical properties, the disadvantage of incorporation of these particles is found in the fabrication process of composites; composites are often fabricated by a powder metallurgical technique (sintering), and dispersed particles hinder densification during sintering [1].

The origins of hindrance in densification must be fully understood to fabricate dense composites with small flaw sizes. Fan and Rahaman summarized the proposed origins of hindrance in a compact containing rigid and inert dispersed-particles [2]; (1) generation of the large viscoelastic backstresses within a matrix, (2) rigid, contiguous network formation by dispersed-particles, (3) crack-like void formation in a matrix, (4) differential sintering caused by non-uniform packing of matrix particles, (5) an anisotropic stress state, and (6) coarsening of matrix particles. However, the experimental results reported in the literature cannot be fully explained by the above origins [1].

It was found that an increase in the volume fraction and a decrease in particle size of dispersed-particles increase the degree of hindrance in densification [3, 4]. Furthermore, the chemical species of matrix and dispersed particles determined the degree of hindrance. For example, (1) the $Zn_7Sb_2O_{12}$, ZrO_2, and aggregated ZnO particles with the same particle size and volume fraction gave the different degree of hindrance in densification of the same ZnO matrix [5], and (2) the same ZrO_2 particles gave a larger hindrance effect on the ZnO matrix than on the Al_2O_3 matrix [6]. Probably, the difference in the formation rate of a neck between matrix and dispersed particles from that between matrix particles is responsible for the hindrance effect. The formation rate of a neck between matrix and dispersed particles is determined by the interaction between matrix and dispersed particles. Thus, the chemical species determines the degree of hindrance.

In this work, Ag and Al_2O_3 were selected for the matrix and dispersed particles, respectively, because the extensive neck formation between Ag and Al_2O_3 is not expected because of the small physical interaction between these materials [7]. Thus, a large hindrance effect is expected. The purposes of this work are (1) to confirm the effect of Al_2O_3 particles on the densification behavior to examine the above expectation and (2) to explain the origin of hindrance effect from the microstructure observation.

We have selected Ag as a matrix, because Ag/Al_2O_3 composites can be heated in air without oxidation. The practical aspect of examining the densification behavior of Ag/Al_2O_3 composites is related to the application to electrodes in multi-layer capacitors [8]. The capacitors are made by co-firing of electrodes and sheets of

a ceramic material. The densification characteristics of the electrode and ceramic material are different, resulting in defects such as delaminations, bowing, blistering, and crazing. To avoid the formation of these defects, dispersed particles are incorporated into the electrode material to minimize shrinkage mismatch. The effects of dispersed particles on the densification behavior and microstructure development must be understood to control the electrode characteristics.

2. Experimental procedure

As-received Ag and Al_2O_3 powders were used without further treatment. Two kinds of Ag, which will be called f-Ag and c-Ag (SP-K1 and SP-EG, respectively, Degussa, Tokyo, Japan), were used as a matrix. The Ag particles were equiaxed and c-Ag had a broad particle size distribution, as observed with a scanning electron microscope (SEM). Fig. 1 shows the SEM photographs of Ag powders. The average particle sizes were 0.3 and 3.0 μm for f-Ag and c-Ag, respectively, as determined from the SEM photographs. Main impurities (more than 30 ppm) were Cu (2000 ppm), K (100 ppm), and NO_3 (50 ppm) for f-Ag and Na (30 ppm) for c-Ag. Four kinds of Al_2O_3, which will be called A0.5, A2, A5, and A15 (Sumi-corundum AA-05, AA-2, AA-5, and AA-18, respectively, Sumitomo Chemical, Osaka, Japan), were used as dispersed particles. Fig. 2 shows the SEM photographs of Al_2O_3 powders. The Al_2O_3 particles were equiaxed and the particle size distribution was small. The average particle sizes were reported to be 0.5, 2.0, 5.0, and 15 μm for A0.5, A2, A5, and A15, respectively, by the manufacturer. Main impurities (more than 10 ppm) were Si (12 ppm) for A2, Fe (15 ppm) and Si (40 ppm) for A5, and Fe (20 ppm) and Si (35 ppm) for A15.

The Ag and Al_2O_3 powders were mixed in a glass beaker with an ultrasonic homogenizer for 5 min, using acetone as a medium. The Al_2O_3 content was 1.0, 5.0, and 20.0 vol% based on the total solid content ($F_i = V_i/(V_m + V_i)$, where F_i is the volume fraction of Al_2O_3, V_m and V_i are the volumes of Ag and Al_2O_3, respectively). The densities used for calculating the volume fraction were 10.53×10^3 and 3.99×10^3 kg/m^3 for Ag and Al_2O_3, respectively. The mixed powders were pressed by cold isostatic pressing. Applied pressure (39–64 MPa) was adjusted to obtain compacts with the matrix relative densities of 50 and 60% for the f-Ag- and c-Ag-matrix composites, respectively. The matrix relative density (ρ_m) is defined by the following equation

$$\rho_m = \frac{V_m}{V_m + V_p}, \tag{1}$$

where V_p is the pore volume.

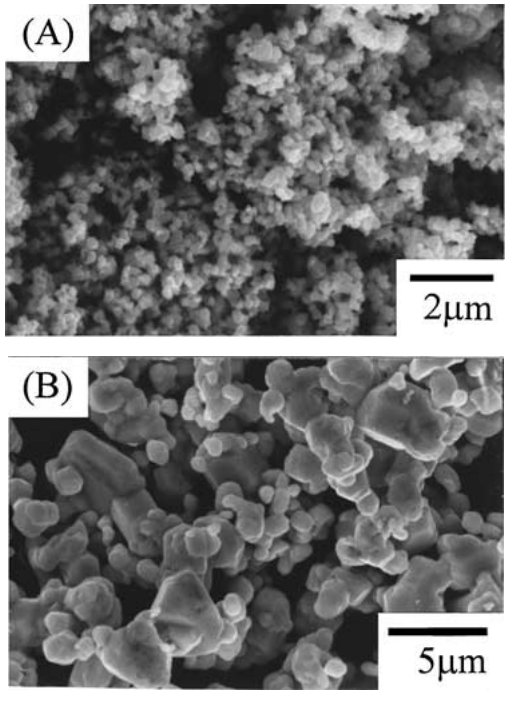

Figure 1 SEM photographs of (A) f-Ag and (B) c-Ag powders.

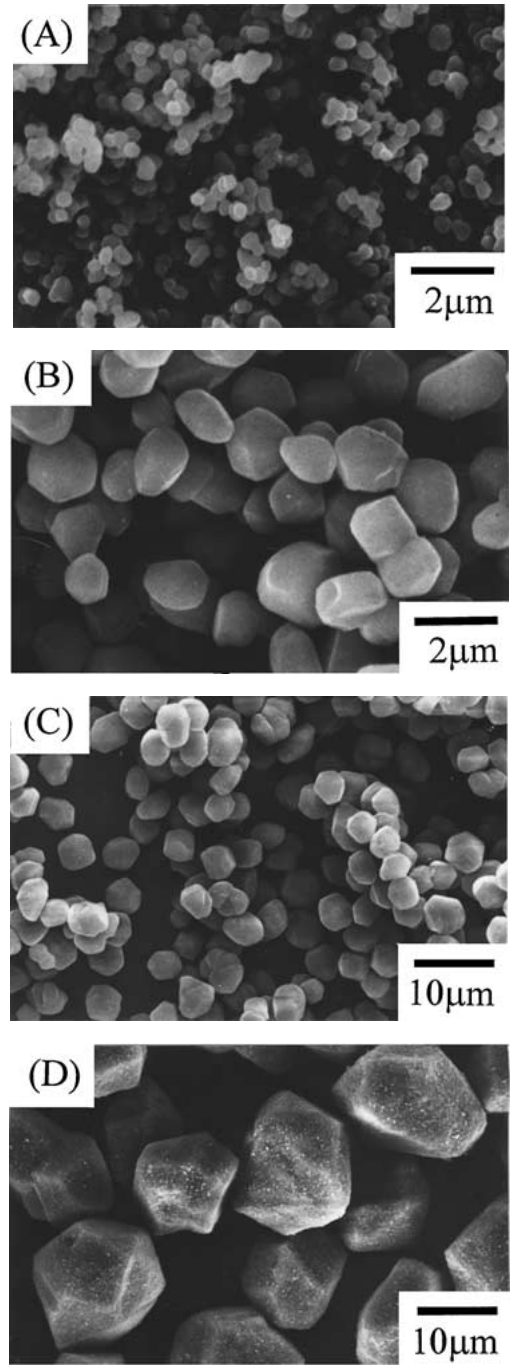

Figure 2 SEM photographs of Al_2O_3 powders; (A) A0.5, (B) A2, (C) A5, and (D) A15.

The densities of the green and sintered compacts were obtained from the weight and size of the compacts. The matrix relative density ρ_m was calculated from the measured density (d_c) using the following relation

$$\rho_m = \frac{d_c(1 - F_i)}{F_i(d_{i,th} - d_c) + d_{m,th}(1 - F_i)}, \qquad (2)$$

where $d_{m,th}$ and $d_{i,th}$ are the theoretical densities of Ag and Al_2O_3, respectively.

Densification behavior was studied by a constant-rate heating (5°C/min) experiment in air. The linear shrinkage was measured with a thermomechanical analyzer (TMA320, Seiko Instruments, Tokyo, Japan). The matrix relative density was calculated from the composite density obtained from the linear shrinkage data assuming isotropic shrinkage. The backscattered electron image of SEM (JSM-5200, JEOL, Tokyo, Japan) was used to observe sections, which were ground, polished, chemically-etched, and sputtered with gold. The sintered compacts were embedded in polyester resin. Uncured resin infiltrated into open pores of the compacts. After curing, resin reinforced the porous compacts for grinding and polishing.

3. Results

3.1. Densification behavior

Fig. 3 shows the densification behavior of pure Ag as well as f-Ag- and c-Ag- matrix composites containing the same content of Al_2O_3 with various particle sizes (20 and 5 vol% for f-Ag- and c-Ag-matrix composites, respectively). The densification behavior of pure f-Ag and c-Ag was different. For f-Ag, densification started at about 280°C and the density increased extensively up to about 350°C. The slope of densification curve changed at about 350°C, and slow densification continued up to about 620°C. Probably, inflection of the densification curve at about 350°C was caused by the change in the dominant densification mechanism. The densification of c-Ag, on the other hand, was monotonous, and it started at about 400°C and the density increased slowly up to 800°C.

The comparison of densification behavior of pure Ag and composites shown in Fig. 3 indicates that the incorporation of Al_2O_3 particles shifts the densification curve downward. This means that the Al_2O_3 particles hinder densification. The smaller Al_2O_3 particles gave greater hindrance. The hindrance was also dependent on the Al_2O_3 content; the higher content gave greater hindrance [9].

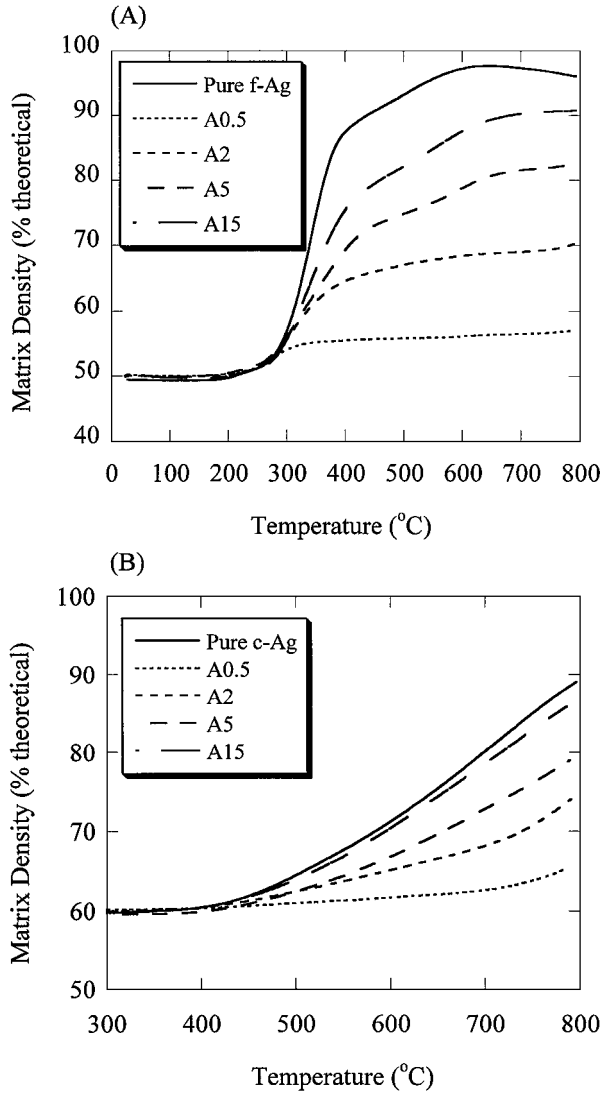

Figure 3 Densification behavior of (A) f-Ag- and (B) c-Ag-matrix composites containing 20 and 5 vol% Al_2O_3, respectively.

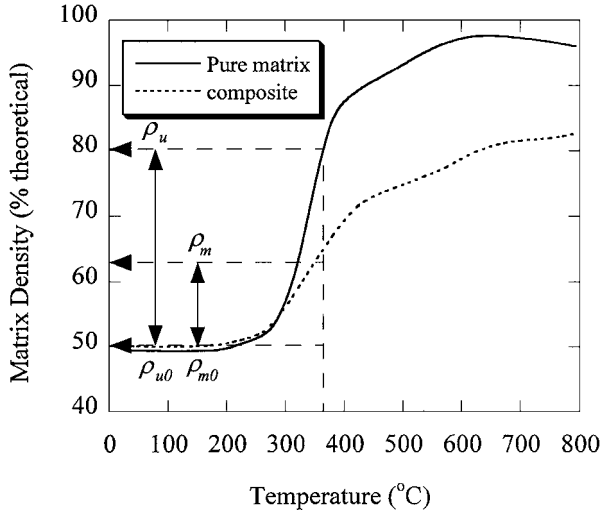

Figure 4 Typical densification curves of pure Ag and a composite and definition of ρ_m, ρ_{m0}, ρ_u, and ρ_{u0}.

3.2. Degree of hindrance

Fig. 4 shows the typical densification curves of pure Ag and a composite. The difference in matrix relative densities of pure Ag and the composite, $\rho_u - \rho_m$, is caused by the hindrance effect of Al_2O_3, where ρ_u and ρ_m are the matrix relative densities of pure Ag and the composite, respectively, heated under the same conditions. The degree of hindrance in densification (D_H) is defined by the following equation

$$D_H = 1 - \frac{\rho_m - \rho_{m0}}{\rho_u - \rho_{u0}}, \qquad (3)$$

where ρ_{u0} and ρ_{m0} are the matrix relative densities of green compacts of pure Ag and the composite,

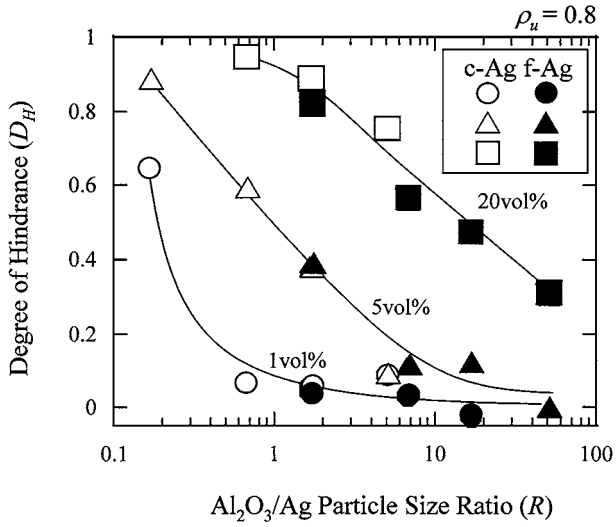

Figure 5 Degree of hindrance (D_H) at $\rho_u = 0.8$ as a function of the Al_2O_3/Ag particle size ratio (R).

respectively. When Al_2O_3 gives no hindrance effect on densification, D_H is zero. When Al_2O_3 fully hinders the densification (no shrinkage in a composite), D_H is unity.

Fig. 5 shows the degree of hindrance in densification at $\rho_u = 0.80$ as a function of the Al_2O_3/Ag particle size ratio (R) for the composites containing 1, 5, and 20 vol% of Al_2O_3. The relation between D_H and R is expressed by a single curve for both f-Ag- and c-Ag-matrix composites with the same Al_2O_3 content. This suggests that the degree of hindrance is determined not independently by the particle size of Ag or Al_2O_3, but by the relative size ratio of Al_2O_3 to Ag. Fig. 5 also indicates the effects of Al_2O_3 particle size and content; a decrease in the Al_2O_3 particle size and an increase in the Al_2O_3 content increase the degree of hindrance.

3.3. Microstructure development of f-Ag-matrix composites

The microstructure development of matrix in the f-Ag-matrix composites with the low number density of Al_2O_3 particles (1 vol% of A0.5, A2, and A5 and 5 vol% of A5 and A15) was almost the same as that of pure f-Ag, except for the regions just surrounding Al_2O_3 particles (we did not examine a composite containing 1 vol% of A15). Fig. 6 shows the microstructures of the composites containing 5 vol% of A5 heated up to 400°, 600°, and 800°C. The light-gray areas are Ag, the large black areas are Al_2O_3 particles, and the small black areas are pores. The comparison of microstructures of the f-Ag-matrix composites with those of pure f-Ag [9] indicates that the shape and distribution of pores in the regions far from A5 particles were not influenced by the presence of A5 particles. However, pores remained around A5 particles at 400°C, and thin circumferential voids formed between matrix and A5 particles at 600° and 800°C.

New microstructural features were observed in the composites with the intermediate number density of Al_2O_3 particles (5 vol% of A0.5 and A2). Fig. 7 shows the microstructures of the composites containing 5 vol% of A0.5 heated up to 400°, 600°, and 800°C. The sintering between Ag particles occurred but the presence of Al_2O_3 particles resulted in the formation of large voids with the elongated shape at 600°C. We will refer these voids to as elongated pores. These elongated pores were not eliminated by further heating and remained at 800°C. In Fig. 7B and C, the elongated pores were filled with resin used for the reinforcement of the compacts, and A0.5 particles were not observed because resin embedded A0.5 particles.

When the number density of Al_2O_3 particles was high (20 vol% of A0.5, A2, and A5), the continuous pores formed in the composites. Figs 8 and 9 show the microstructures of the composites containing 20 vol% of A0.5 and A5, respectively. In the case of A0.5, elongated pores containing A0.5 particles were connected by increasing the amount of A0.5 form 5 to 20 vol% (compare Fig. 7 with Fig. 8) and the connectivity of matrix Ag was lost. We will refer the continuous pores to as pore channels and well-sintered regions of Ag to as domains. The size of domains increased from 600° to 800°C, but the thickness of pore channels also increased. In the case of A5, the length of pore channels

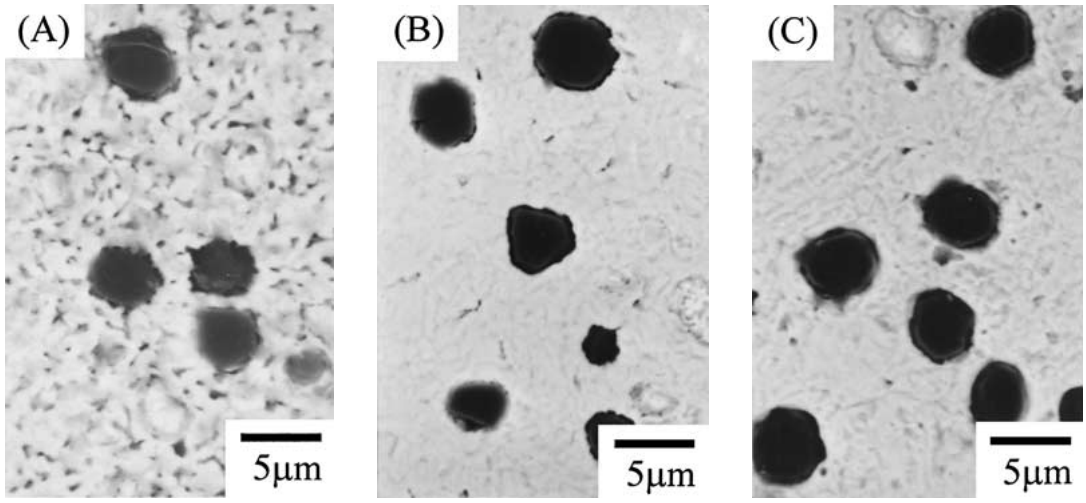

Figure 6 Microstructures of f-Ag-matrix composites containing 5 vol% of A5, heated up to (A) 400°, (B) 600°, and (C) 800°C.

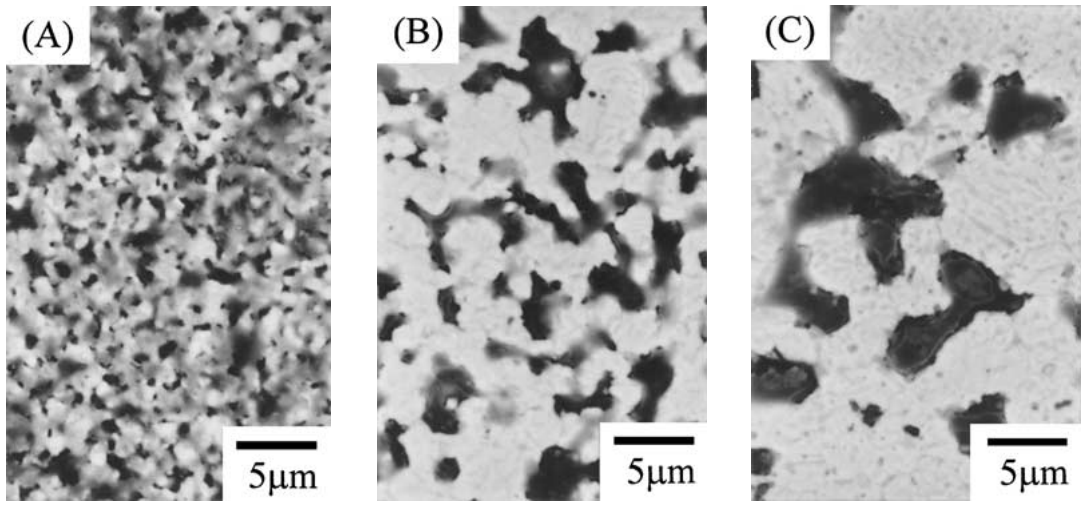

Figure 7 Microstructures of f-Ag-matrix composites containing 5 vol% of A0.5, heated up to (A) 400°, (B) 600°, and (C) 800°C.

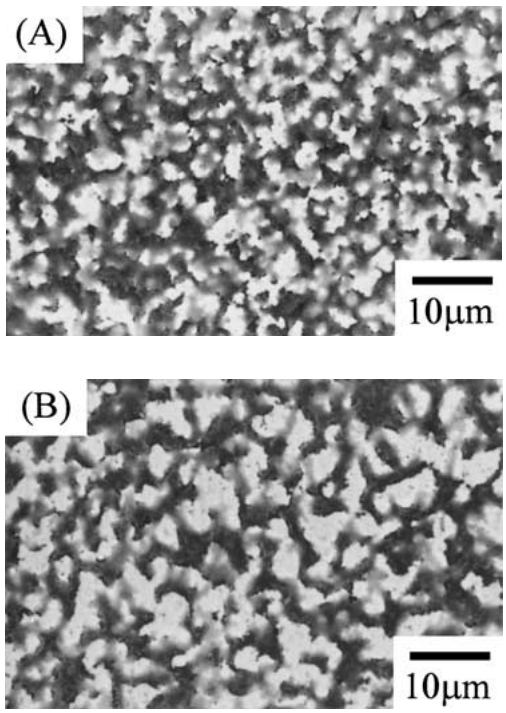

Figure 8 Microstructures of f-Ag-matrix composites containing 20 vol% of A0.5, heated up to (A) 600° and (B) 800 °C.

was shorter than that in the composite containing A0.5, and the extent of reduction in the connectivity of Ag matrix was smaller.

Pore channels did not form in the composite containing 20 vol% of A15, and A15 particles were isolated from other A15 particles (Fig. 10). In this case, another microstructural feature was observed. The density of matrix Ag was not uniform but dense regions developed between A15 particles with close separations at 400°C. At 600°C, the non-uniformity of density disappeared, but pores in the matrix were present (only a few pores remained in pure f-Ag at 600°C).

3.4. Microstructure development of c-Ag-matrix composites

The incorporation of a small amount (1 vol%) of Al_2O_3 did not change the microstructural features of c-Ag. Fig. 11 shows the microstructures of the composites containing 1 vol% of A0.5 and A5 heated up to 700°, 800°, and 900°C. Pore size was larger than that of the f-Ag-matrix composites (Fig. 6) and pore shape was irregular and elongated as shown in Fig. 11A, B, and D. The elongated pores were present up to 700°C in pure c-Ag and changed to isolated, equiaxed pores at 800°C [9]. The incorporation of Al_2O_3 increased the temperature at which the elongated pores disappeared; the elongated pores remained up to 800°C in the composites, and the pore volume was dependent on the size of Al_2O_3 particles. A large fraction of pores with an irregular shape was observed around A5 particles (Fig. 11D and E).

When the composites containing 5 vol% of Al_2O_3 were heated, the elongated pores remained up to 900°C for A0.5 and A2, 800°C for A5, and 700°C for A15. Fig. 12 shows the typical microstructures. For the composite containing A0.5, continuous pores (pore channels) existed at 800°C, and they changed to elongated pores at 900°C. For the composites containing A15, the elongated pores were still present in the matrix at 800°C whereas pure c-Ag contained no elongated pores at the same temperature. Large, irregularly shaped pores remained around A15 particles up to 800°C but these pores were eliminated at 900°C.

When the composites containing 20 vol% of A2, A5, and A15 were heated, elongated pores and pore channels remained up to 900°C (we did not examine a composite containing A0.5). Fig. 13 shows the microstructures of the composites obtained at 900°C. In the cases of A2 and A5, the Al_2O_3 particles formed long pore channels. In the case of A15, the pores around A15 particles remained up to 900°C, and the distance between A15 particles determined the pore shape. When the distance was large, an A15 particle was isolated and irregularly shaped pores remained around the particle. When the distance was small, pores between particles as well as pores around particles remained. Thus, several A15 particles with close separation formed a group of A15 particles with pores between particles and irregularly-shaped pores around it.

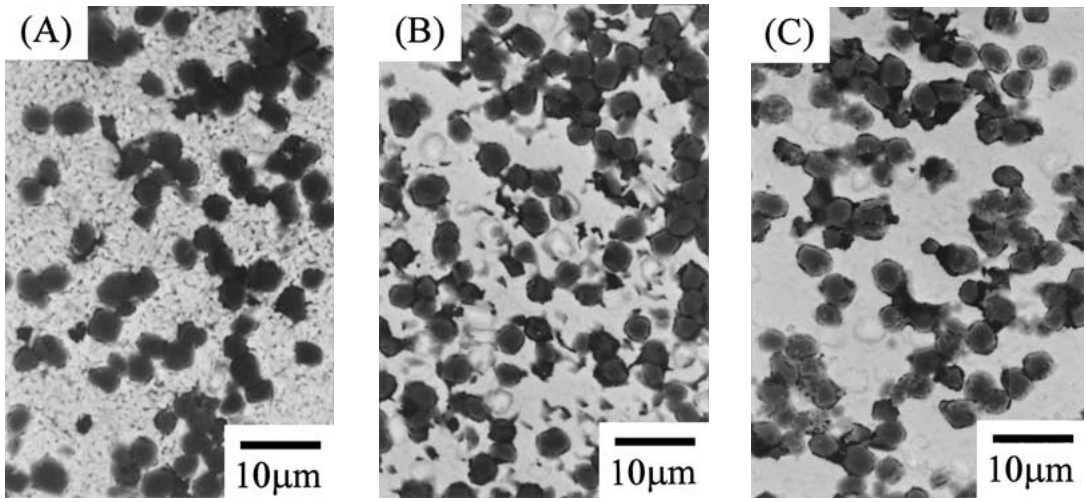

Figure 9 Microstructures of f-Ag-matrix composites containing 20 vol% of A5, heated up to (A) 400°, (B) 600°, and (C) 800°C.

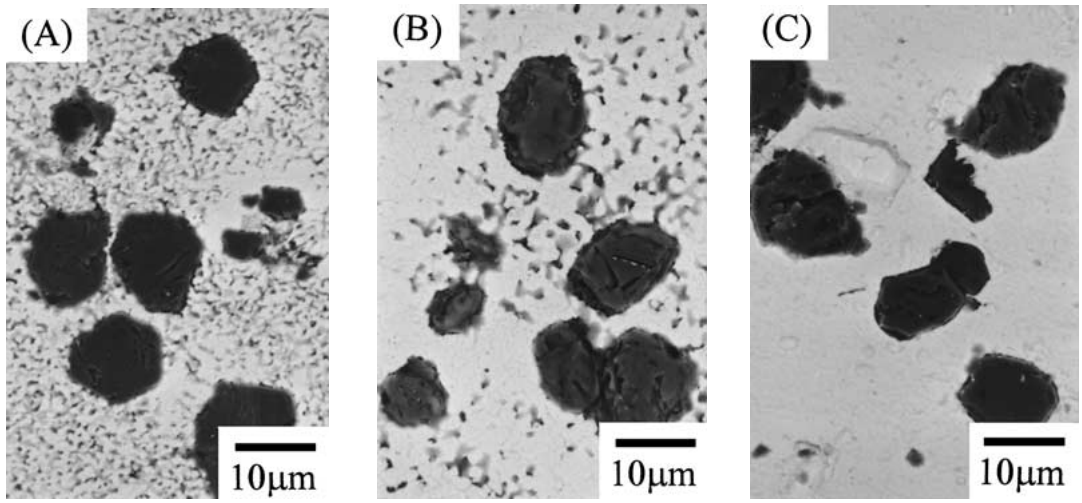

Figure 10 Microstructures of f-Ag-matrix composites containing 20 vol% of A15, heated up to (A) 400°, (B) 600°, and (C) 800°C.

4. Discussion

4.1. Microstructural characteristics

The incorporation of Al_2O_3 particles into Ag created microstructures different from those of pure Ag. These microstructures had three characteristics; (1) pores around an Al_2O_3 particle (Figs 6, 10, 11E, 12C, D, and 13C), (2) elongated pores (Figs 7, 9, and 13C) and pore channels (Figs 8, 12A, B, 13A, and B), and (3) dense regions of matrix between Al_2O_3 particles (Fig. 10A). These microstructural features are the origins of hindrance in densification.

4.1.1. Pores around an Al_2O_3 particle

The pores around an Al_2O_3 particle formed, when the number density of Al_2O_3 particles was low and an Al_2O_3 particle was isolated from other Al_2O_3 particles. The origin of these pores is the small rate of Ag transport to the region of contact between Ag and Al_2O_3 particles, as suggested from small physical interaction between Ag and Al_2O_3 [7]. Although the bonding between Ag and Al_2O_3 is expected by the solid state bonding in air [10], a large extent of necks between Ag and Al_2O_3 did not develop in the present case, as suggested by the formation of circumferential voids. Probably, the absence of pressure and low sintering temperature result in the lack of a large extent of necks.

In a green compact, there are two kinds of particle-to-particle contacts; between Ag particles and between Ag and Al_2O_3 particles. When the compact is heated, necks between Ag particles form at an earlier stage than those between Ag and Al_2O_3 particles, and pores around an Al_2O_3 particle remain. These pores are large and the rate of elimination is small, and therefore they remain up to high temperatures, at which the densification of pure Ag is almost completed.

In the f-Ag-matrix composites, the size of pores around an Al_2O_3 particle is small compared to that in the c-Ag-matrix composites, and the surface of pores is rough at low temperatures (Figs 6A and 10A). The transport of Ag is enhanced at high temperatures by surface diffusion or evaporation-condensation. This changes the morphology of pore surface, i.e., the pore surface facing to an Ag particle becomes smooth, forming a circumferential void (Figs 6B and 10C).

In the c-Ag-matrix composites, the size of pores around an Al_2O_3 particle is large and their shape is irregular (Figs 11D and 12C). In this case, surface diffusion or evaporation-condensation cannot create circumferential voids. At 900°C, grain growth occurred

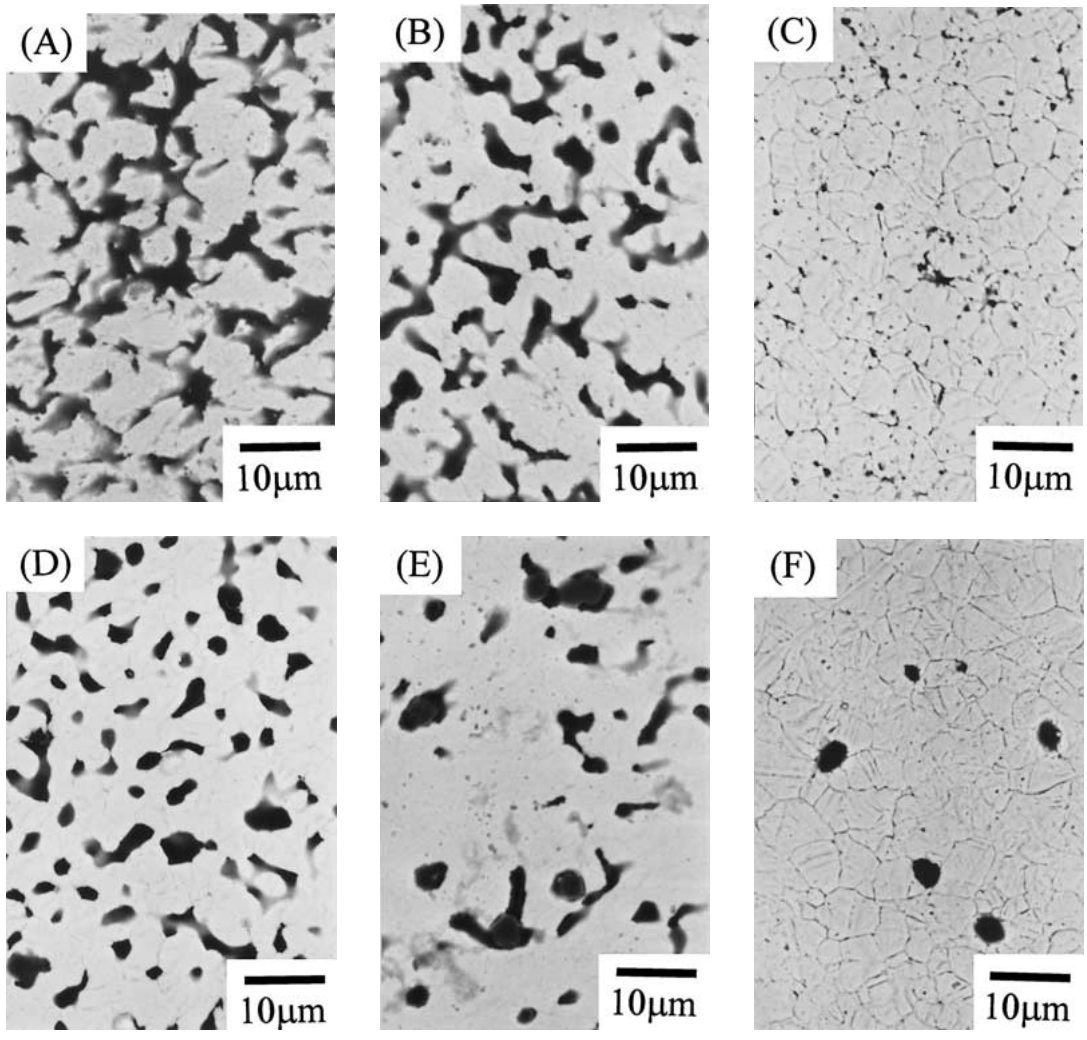

Figure 11 Microstructures of c-Ag-matrix composites containing 1 vol% of (A), (B), and (C) A0.5 and (D), (E), and (F) A5, heated up to (A) and (D) 700°, (B) and (E) 800°, and (C) and (F) 900°C.

extensively, and pores around an isolated Al_2O_3 particle were eliminated (Figs 11F and 12E). The stability of pore is related to the pore size to grain size ratio [11]. The instability of pores becomes large with extensive grain growth, and these pores are eliminated at 900°C in the c-Ag-matrix composites.

The pores around Al_2O_3 particles are one of the origins of the hindrance in densification, because these pores remain up to high temperatures. However, because an isolated Al_2O_3 particle did not influence the microstructure development of the major part of matrix phase (far from Al_2O_3 particles), the hindrance effect was small in the composites containing the low number density of Al_2O_3 particles.

4.1.2. Elongated pores and pore channels

When the number density of Al_2O_3 particles is intermediate, the distance between Al_2O_3 particles becomes small, the pores around a few Al_2O_3 particles are connected, and elongated pores containing a few Al_2O_3 particles develop. We will refer a group of Al_2O_3 particles in the elongated pore to as a cluster. Figs 9 and 13C show the typical microstructure of clusters. In this case, the connectivity of Ag matrix particles is not lost. Thus, densification can occur by shrinkage in the matrix. However, the formation of clusters results in a decrease in densification rate, because the pore volume within and around a cluster is more than the sum of the pores around Al_2O_3 particles, which consist of the cluster. Thus, clusters give a larger hindrance effect than isolated Al_2O_3 particles.

When the number density of Al_2O_3 particles is further increased, the number and size of clusters become large and clusters come in contact with each other. In this case, the clusters form pore channels, and the connectivity of matrix phase is lost. The shrinkage within isolated matrix domains causes the growth of the thickness of pore channels, leading to no or small shrinkage of the overall compact. Thus, the formation of continuous pore channels results in the largest hindrance effect on densification.

4.1.3. Dense regions between Al_2O_3 particles

Dense regions between Al_2O_3 particles were observed when a large amount of large Al_2O_3 particles (A15) was incorporated into matrix of small particles (f-Ag) (Fig. 10A). This kind of microstructure was found in the Al_2O_3- and ZnO-matrix composites with ZrO_2 particles [12, 13]. In these systems, the dense regions developed with the combination of small matrix particles and large inclusion particles, as in the present experiment. The

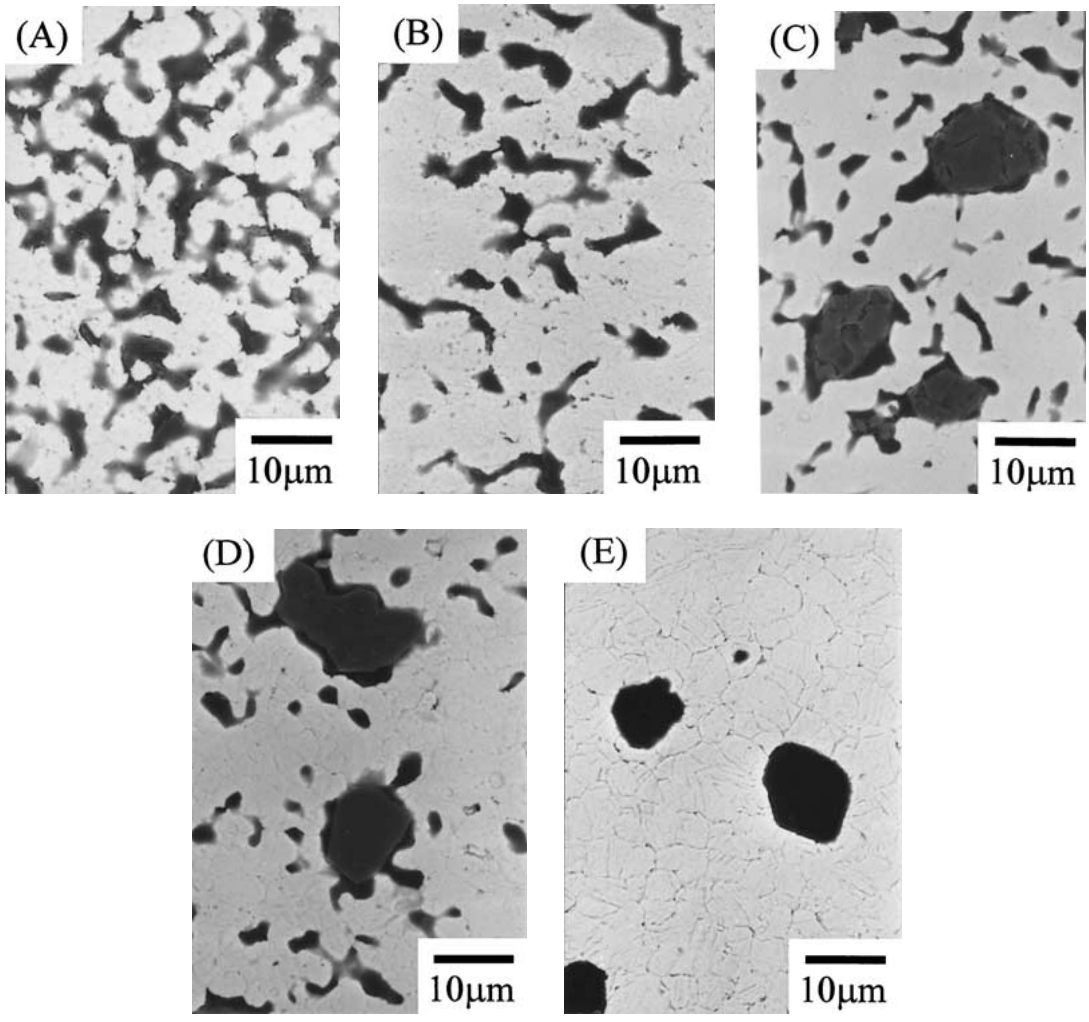

Figure 12 Microstructures of c-Ag-matrix composites containing 5 vol% of (A) and (B) A0.5 and (C), (D), and (E) A15, heated up to (C) 700°, (A) and (D) 800°, and (B) and (E) 900 °C.

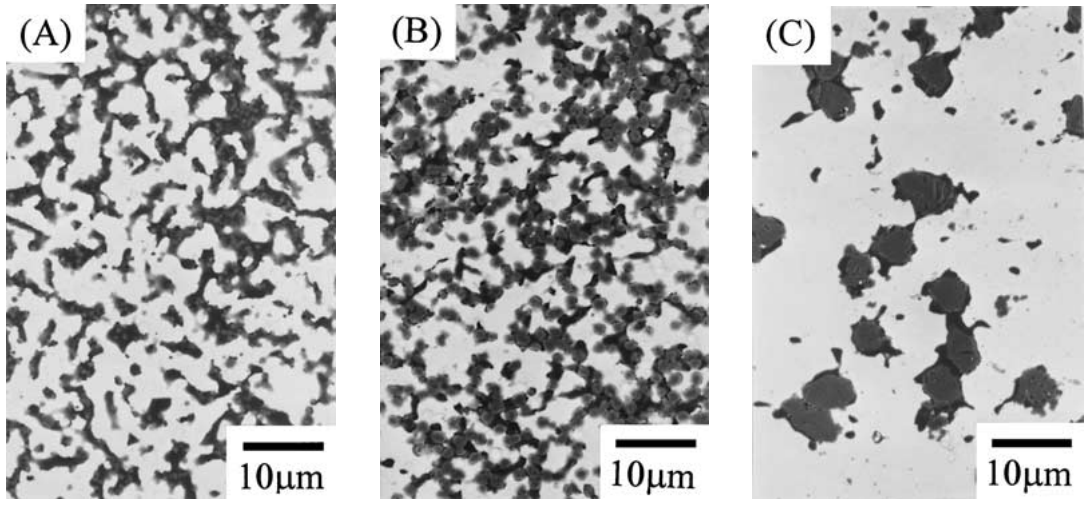

Figure 13 Microstructures of c-Ag-matrix composites containing 20 vol% of (A) A2, (B) A5, and (C) A15 heated, heated up to 900°C.

stress development in the matrix phase is proposed for the formation of the dense regions [14].

The microstructures at 600° and 800°C shown in Fig. 10 indicate the absence of non-uniformity of density between A15 particles with small distances. This means that the network made by A15 particles and dense matrix regions is not rigid, and densification continues in the regions surrounded by the network. However, pores are almost eliminated in pure f-Ag at 600°C [9], but pores in the matrix phase remained in the composite (Fig. 10B). This means that the network reduces the densification rate of matrix [15].

4.2. Effect of particle size ratio

The Al_2O_3/Ag particle size ratio determined the degree of hindrance of the composites with the same Al_2O_3

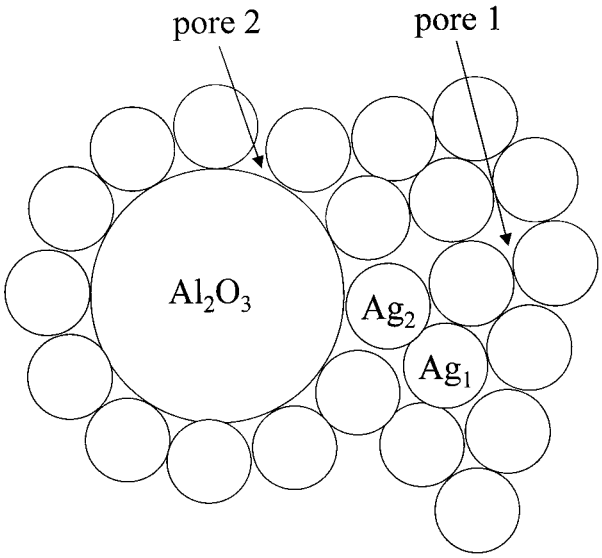

Figure 14 Two-dimensional packing of Ag particles around an Al_2O_3 particle. Ag_1 is Ag particle surrounded by Ag particles and Ag_2 is an Ag particle coordinating to Al_2O_3. Pore 1 locates between matrix Ag particles, and pore 2 is the pores around an Al_2O_3 particle.

content (Fig. 5). To explain the effect of particle size ratio, it is assumed that pores surrounded by only Ag particles can shrink but those touching Al_2O_3 particles cannot shrink by sintering. This simple assumption can derive a relation between the degree of hindrance and the particle size ratio, based on a simple model [16].

The ratio of total volume of pores touching Al_2O_3 particles to that of pores in a green compact is first calculated. Fig. 14 shows the two-dimensional packing model of Ag (matrix) particles around an Al_2O_3 (inclusion) particle. The model assumes that pores 1 surrounded by matrix particles can be eliminated, but pores 2 surrounded by inclusion and matrix particles remain. Therefore, the relation between the particle size ratio and the ratio of the total volume of pores 2 to that of pores 1 and 2 is examined.

We consider a green compact of composite composed of N_m matrix and N_i inclusion particles with the radii of r_m and r_i, respectively. Fig. 15 shows the total volume of matrix (V_m), inclusions (V_i), and pores (V_{p0}) in the green compact. $V_{p0,1}$ and $V_{p0,2}$ are the total volume of pores 1 and 2, respectively. The total volume of matrix

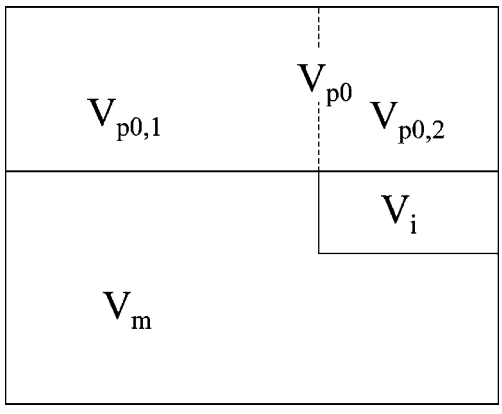

Figure 15 Volume of matrix (V_m), inclusions (V_i), and pores (V_{p0}) in a green compact. $V_{p0,1}$ and $V_{p0,2}$ are the volume of pores surrounded by matrix particles and around inclusion particles, respectively ($V_{p0,1} + V_{p0,2} = V_{p0}$).

and inclusion particles is obtained from N_m and N_i.

$$V_m = \frac{4}{3}\pi r_m^3 N_m \tag{4}$$

$$V_i = \frac{4}{3}\pi r_i^3 N_i \tag{5}$$

In the experiment, the volume fraction of inclusions (F_i) was defined based on the total solid content ($F_i = V_i/(V_m + V_i)$) and the matrix green density (ρ_{m0}) was defined as $\rho_{m0} = V_m/(V_m + V_{p0})$. Therefore, the total volume of inclusion particles and pores is related to the total volume of matrix particles by the following equation.

$$V_i = \frac{F_i}{1 - F_i} V_m \tag{6}$$

$$V_{p0} = \frac{1 - \rho_{m0}}{\rho_{m0}} V_m \tag{7}$$

From Equations 4–6, the number of inclusion particles is related to that of matrix particles.

$$N_i = \left(\frac{F_i}{1 - F_i}\right)\left(\frac{r_m}{r_i}\right)^3 N_m \tag{8}$$

To obtain the total volume of pores 2, the pore volume touching one inclusion particle is calculated first. It is obtained from the number of pores touching one inclusion particle (n_{p2}) multiplied by the volume of each pore (v_{p2}). The number of pores is proportional to the coordination number of an inclusion particle, and the coordination number (N_C) is related to the particle size ratio by the following equation [17].

$$N_C = 3.0 + 3.16\left(\frac{r_i}{r_m}\right)^2 \tag{9}$$

Thus, we assume that N_C and the number of pores touching one inclusion particle are proportional to $(r_i/r_m)^2$ for simplicity.

$$n_{p2} \propto \left(\frac{r_i}{r_m}\right)^2 \tag{10}$$

To obtain v_{p2}, we assume that the volume of pore 2 (v_{p2}) is proportional to that of pore 1 (v_{p1}) and v_{p1} is proportional to the pore volume per matrix particle, which is obtained by dividing the total pore volume (V_{p0}) by the total number of matrix particles (N_m) and by using Equations 4 and 7.

$$v_{p2} \propto v_{p1} \propto \frac{V_{p0}}{N_m} = \frac{\{(1 - \rho_{m0})/\rho_{m0}\}V_m}{N_m} = \left(\frac{1 - \rho_{m0}}{\rho_{m0}}\right)\left(\frac{4}{3}\pi r_m^3\right) \tag{11}$$

The combination of Equations 10 and 11 gives that the pore volume around one inclusion particle is proportional to $\{(1 - \rho_{m0})/\rho_{m0}\}r_i^2 r_m$.

The total pore volume touching inclusion particles ($V_{p0,2}$) is obtained from the number of inclusion particles (N_i) and the pore volume touching an inclusion particle and using Equation 8.

$$V_{p0,2} \propto N_i \left(\frac{1-\rho_{m0}}{\rho_{m0}}\right) r_i^2 r_m$$
$$= \left(\frac{F_i}{1-F_i}\right)\left(\frac{r_m}{r_i}\right)^3 N_m \left(\frac{1-\rho_{m0}}{\rho_{m0}}\right) r_i^2 r_m$$
$$= \left(\frac{F_i}{1-F_i}\right)\left(\frac{1-\rho_{m0}}{\rho_{m0}}\right)\left(\frac{r_m^4}{r_i}\right) N_m \qquad (12)$$

The hindrance is related to the ratio of the total volume of pores touching inclusions ($V_{p0,2}$) to that of pores in the compact (V_{p0}). From Equations 4, 7, and 12, we obtain the following equation.

$$\frac{V_{p0,2}}{V_{p0}} \propto \left(\frac{F_i}{1-F_i}\right)\left(\frac{r_m}{r_i}\right) \qquad (13)$$

This relation indicates that the degree of hindrance is dependent on the particle size ratio for composites with fixed F_i.

4.3. Calculation of D_H

4.3.1. Model

The degree of hindrance may be calculated using Equation 13 by assuming an appropriate proportionality constant. However, the above model considers only pores touching inclusion particles surrounded by matrix particles and does not consider pores between inclusion particles. The pores between inclusion particles formed when the clusters and pore channels developed.

The distribution of pores surrounded by spheres with two radii can be calculated using the model proposed by Dodds [18]. The model is based on the gapless packing of multicomponent particles. The packing is divided up into tetrahedral subunits shown in Fig. 16 and the frequency of the tetrahedral subunits (F_{qrst}) can be calculated (the calculation method is shown in the Appendix). In the present case, there are five kinds of subunits which are composed of *mmmm*, *mmmi*, *mmii*, *miii*, and *iiii*, where *m* and *i* stand for matrix and inclusion particles at the apexes of tetrahedral subunit.

Each tetrahedral subunit has its own characteristic pore volume (v_{qrst}) which is calculated from Equations A4 and A5. The overall relative pore volume of each subunit is given by the pore volume of each subunit multiplied by the relative frequency; $V_{qrst} = v_{qrst} \times F_{qrst}$.

We assume that pores in the subunit *mmmm* can be eliminated by sintering, but the pores in the subunits *mmmi*, *mmii*, *miii*, and *iiii* remain. The values of V_{mmmm} and $\Sigma(V_{mmmi} + V_{mmii} + V_{miii} + V_{iiii})$ are calculated. The Dodds' model is based on the gapless packing. So the porosity calculated for packing of monosized spheres is 22.04%. This value is too small compared to 36.3 and about 40% for the random dense and random loose packings. So, the volume of pores surrounded by matrix particles ($V_{p0,1}$) and that of pores touching inclusion particles ($V_{p0,2}$) are calculated by the following

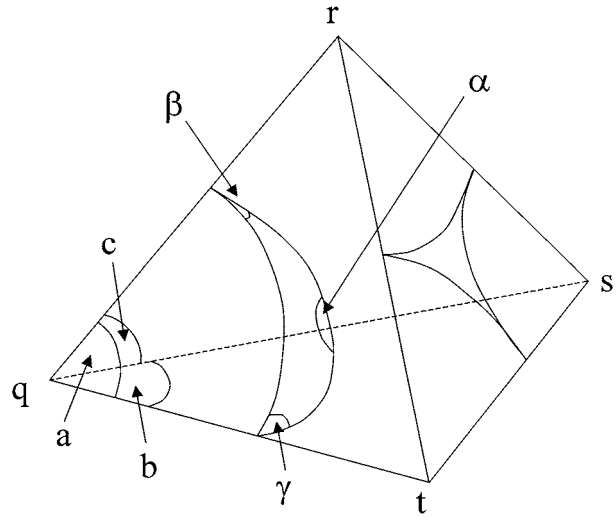

Figure 16 Tetrahedral subunit made by spheres q, r, s, and t. Marks a, b, and c indicate the angles of triangles, and α, β, and γ indicate the spherical angles.

equations.

$$V_{p0,1} = \frac{V_{mmmm}}{V_{mmmm} + \sum(V_{mmmi} + V_{mmii} + V_{miii} + V_{iiii})} V_{p0} \qquad (14)$$

$$V_{p0,2} = \frac{\sum(V_{mmmi} + V_{mmii} + V_{miii} + V_{iiii})}{V_{mmmm} + \sum(V_{mmmi} + V_{mmii} + V_{miii} + V_{iiii})} V_{p0} \qquad (15)$$

The degree of hindrance (D_H) is defined by Equation 3. The experimental values of D_H were obtained at $\rho_u = 0.8$. The green compacts had $\rho_{u0} = \rho_{m0} = 0.5$ and 0.6 for f-Ag- and c-Ag-matrix composites, respectively. The total volume of matrix particles (V_m), inclusion particles (V_i), and pores (V_p) in a sintered compact is shown in Fig. 17. The matrix relative density is calculated by $\rho_m = V_m/(V_m + V_p)$ in the experiment. We assume that pores surrounded only by Ag particle

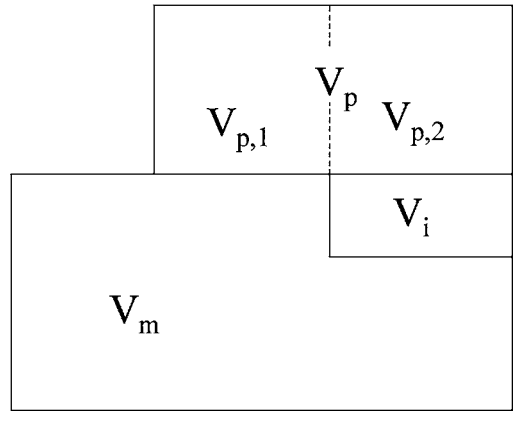

Figure 17 Volume of matrix (V_m), inclusions (V_i), and pores (V_p) in a sintered compact. $V_{p,1}$ and $V_{p,2}$ are the volume of pores surrounded by matrix particles and around inclusion particles, respectively.

TABLE I Values used for the calculation

Volume fraction of inclusion (F_i)	0.01	0.05	0.20			
Particle size ratio (r_i/r_m)	0.167	0.667	1.67	5.00	6.67	50.0
Matrix green density (ρ_{m0}, ρ_{u0})	0.50	0.60				
Sintered density of pure Ag (ρ_u)	0.80					

densify in the same manner in pure Ag and composites. Thus, $V_m/(V_m + V_{p,1})$ is 0.8 in a sintered composite at the experimental conditions under which ρ_u reaches 0.8.

$$V_{p,1} = 0.25V_m \tag{16}$$

The matrix relative density for a sintered composite is given by the following relation.

$$\rho_m = \frac{V_m}{V_m + V_{p,1} + V_{p0,2}} \tag{17}$$

By using Equations 7, 15, and 16, we obtain ρ_m. Thus, the D_H value can be obtained from Equation 3.

4.3.2. Calculation

Table I shows the data used for the calculation. These values were determined from the experimental conditions. The calculation based on the Dodds' method is applicable to the particle size range between 1/6.46 (0.155) and 6.46. If the particle size ratio is out of this range, the tetrahedral subunit made of three large spheres and one small sphere is not composed; the small sphere can contact with only two large spheres. The ratios of the particle size of Al_2O_3 to that of Ag are 16 and 50 for f-Ag-matrix composites containing A5 and A15 particles, respectively. In these cases, we assumed that the *miii* tetrahedral subunit was absent.

Fig. 18 shows the calculated and experimental values of D_H as a function of the particle size ratio (R) of Al_2O_3 to Ag. The calculated relation between D_H and R qualitatively coincided with the experimental values. The relation for f-Ag- and c-Ag-matrix composites with the same Al_2O_3 content could be expressed by a single curve. This indicates that the particle size ratio is a decisive factor in determining the degree of hindrance. However, the calculation underestimated the D_H values.

4.3.3. Discrepancy between calculated and observed D_H

The discrepancy between the calculated and observed D_H values can be explained from the microstructural observation. Possible origins are packing inhomogeneity, migration of Al_2O_3 particles, differential sintering, breaking of matrix connectivity, hindrance by inclusion particles, and Ostwald ripening of pores.

4.3.3.1. Packing inhomogeneity. The present model assumes homogeneous distribution of matrix particles throughout a compact. In practice, the incorporation of inclusion particles reduces the homogeneity of matrix particle packing [2, 17]. It is expected that packing density in regions immediately surrounding inclusion particles is lower than that in regions far from inclusion particles, because larger applied pressure was necessary

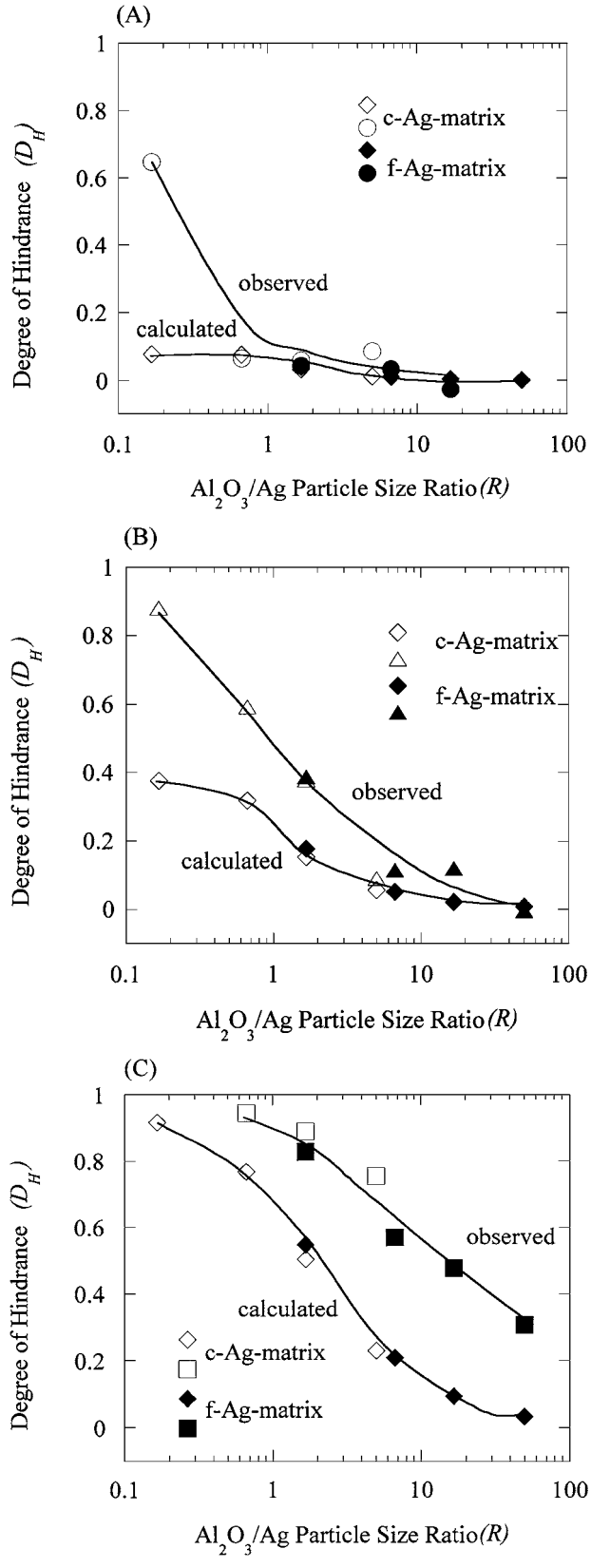

Figure 18 Calculated D_H values as a function of particle size ratio ratio in the composites containing (A) 1, (B) 5, and (C) 20 vol% of Al_2O_3. Observed D_H values are also shown.

to obtain the compacts with the same matrix density for the composites with the higher Al_2O_3 content. The calculated total volume of pores 2 may be smaller than the actual total volume of pores touching Al_2O_3 particles.

4.3.3.2. Migration of Al_2O_3 particles. The calculated D_H values were obtained by assuming that initial particle distribution did not change during densification. However, migration of Al_2O_3 particles is possible. It is exemplified from the microstructures of the f-Ag-matrix composites containing 5 vol% of A0.5 (Fig. 7). The distribution of A0.5 particles in the green compact was uniform, as judged from the microstructure shown in Fig. 7A. However, the absence of A0.5 particles in the matrix phase (Fig. 7B and C) indicates that A0.5 particles were accumulated in pore channels. The neck formation as well as the development of grain boundary between two Ag particles expels A0.5 particles from the contact area between the Ag particles, resulting in the accumulation of A0.5 particles which form pore channels.

The migration of Al_2O_3 particles, which forms clusters and pore channels, changes pore 1 to pore 2 and increases the volume of pore 2 during sintering, resulting in the larger D_H value than the calculated one.

4.3.3.3. Differential sintering. Weiser and De Jonghe [19] showed that pores in the regions with densely packed particles shrank but those in the regions with loosely packed particles opened up. In the present composites, pores touching Al_2O_3 particles correspond to the regions with loosely packed particles. We assume in the calculation that the shrinkage of pores 1 in Fig. 14 results in the densification of compact. However, the neck between Ag_2 and Al_2O_3 particles does not form, when the neck between Ag_1 and Ag_2 particles forms. The neck formation reduces the distance between Ag_1 and Ag_2 particles, and moves the Ag_2 particle apart from the Al_2O_3 particle. Thus, reduction in the volume of pore 1 partly results in an increase in the volume of pore 2, and the shrinkage of pore 1 does not fully contribute to the overall shrinkage of the compact. This mechanism is operative in all composites irrespective of the Al_2O_3 content.

4.3.3.4. Breaking of matrix connectivity. When the number density of Al_2O_3 was high, the pore channels formed. In this case, the connectivity of Ag particles was lost. Pores in a group of Ag particles (domain) surrounded by pore channels may shrink. However, the shrinkage in the domain causes only thickening of pore channels and does not contribute to the overall shrinkage of the compact. This is a similar situation to the sintering of bimodal powder compact containing a sphere which shrinks faster than the matrix surrounding the sphere [20].

4.3.3.5. Hindrance in densification by the presence of inclusion particles. Fig. 19 shows the microstructures of pure c-Ag and composites containing 1, 5, and 20 vol% of A15 particles, heated up to 800°C. At this temperature, pores in pure c-Ag were isolated

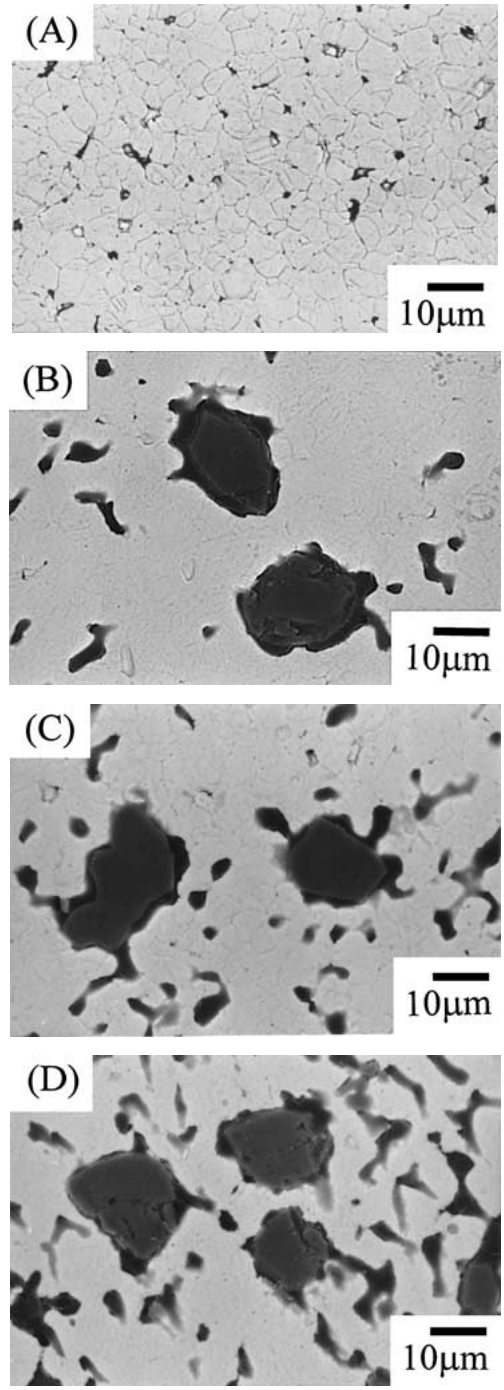

Figure 19 Microstructures of (A) pure c-Ag and c-Ag-matrix composites containing (B) 1, (C) 5, and (D) 20 volume% of A15 particles, heated up to 800°C.

and equiaxed. For the composites, however, elongated, irregularly shaped pores remained in the regions far form Al_2O_3 particles, and the amount of these pores increased as the volume fraction of Al_2O_3 particles increased. These pores are surrounded by only Ag particles in the green compact and assumed to be eliminated as in pure c-Ag in the calculation of the D_H values. However, the shape of pores indicates that the rate of elimination of pores in the composites is smaller than that in pure c-Ag. This implies that the presence of inclusion particles reduces the densification rate of matrix regions.

Fig. 19 indicates that the Ag matrix is continuous and the reduction in densification rate is caused at the

regions far from Al_2O_3 particles. Thus, the mechanism other than that mentioned above must be operative. The generation of the transient stresses within a matrix is ruled out to explain the reduction in densification rate because the predicted stresses are significantly small [1].

The shrinkage of matrix adjacent to an inclusion particle is not isotropic; the shrinkage parallel to the interface between the inclusion and matrix is suppressed by the presence of the inclusion particle, as observed in the sintering of film on a substrate [21]. This anisotropic shrinkage is one of the origins of reduction in densification rate [6].

4.3.3.6. Ostwald ripening. Another possible mechanism is the pore growth by the Ostwald ripening [22]. The shrinkage rate of pores around Al_2O_3 particles is smaller than that of pores in the matrix. This results in the co-existence of large and small pores. Material transport from the surface of large pores to that of small pores results in the growth of large pores, and reduces the densification rate.

4.4. Inflection in the densification curves of f-Ag-matrix composites

The inflection was observed in the densification curves of pure f-Ag and the f-Ag-matrix composites (Fig. 3A). The temperature of the inflection was constant irrespective of the Al_2O_3 content and Al_2O_3 particle size, but the matrix relative density at the inflection point decreased as the Al_2O_3 content increased and the Al_2O_3 particle size decreased. This means that the incorporation of Al_2O_3 particles does not change the temperature range, at which a specific densification mechanism is dominant.

If Al_2O_3 particles develop stresses in the matrix as proposed by Raj and Bordia [20] and Scherer [23], the Al_2O_3 particles reduce the driving force for densification. This predicts the shift of the inflection point to higher temperatures, which is opposed to the experimental results. Thus, the development of stresses in the matrix is ruled out to explain the major origin of the hindrance in densification for the present system.

5. Conclusions

The incorporation of Al_2O_3 particles into the Ag matrix hindered the densification of matrix. The degree of hindrance (D_H) in densification of Ag/Al_2O_3 composites was determined not independently by the particle size of Ag or Al_2O_3, but by the relative size ratio of Al_2O_3 to Ag. The microstructure observation revealed that the major origin of the hindrance effect was the formation of large pores around Al_2O_3 particles, clusters of Al_2O_3 particles, and pore channels. When the number density of Al_2O_3 particles was low and Al_2O_3 particles were isolated, the matrix far from Al_2O_3 particles densified but pores remained around Al_2O_3 particles, for which the small physical interaction between Al_2O_3 and Ag was responsible. When the number density of Al_2O_3 particles was intermediate, pores around Al_2O_3 particles were connected and the clusters made of a few Al_2O_3 particles formed, and pores within and around clusters remained up to high temperatures. When the number density of Al_2O_3 particles was high, the connection of clusters resulted in the formation of pore channels. The three-dimensional connectivity of Ag was decreased, and the shrinkage between Ag particles resulted in the growth of pore channels. Thus, pore channels gave a severe hindrance effect on densification.

The effect of the relative size ratio on the degree of hindrance was explained by assuming that the pores around Al_2O_3 particles were not eliminated. The calculation of the D_H value using a packing model of bimodal mixtures of spherical particles gave a qualitative relation between D_H and R. This result indicates that the major origin of hindrance in densification is the difficulty in eliminating pores around Al_2O_3 particles. Quantitatively, however, the calculated values were smaller than the observed values. This discrepancy is caused by (1) packing inhomogeneity, (2) migration of Al_2O_3 particles, (3) differential sintering, (3) breaking matrix connectivity, (4) hindrance in densification by the presence of inclusion particles, and (5) Ostwald ripening.

Acknowledgment

We would like to thank Sumitomo Chemical Co., Ltd. for the supply of Al_2O_3 powder (Sumi-corundum series).

Appendix: Calculation of pore volume

The frequency distribution of tetrahedron subunits is calculated as described by Dodds [18]. However, his paper contained several errors in the expression of equations. So, the procedure of calculation is briefly outlined.

In the tetragonal subunit shown in Fig. 16 formed by spheres q, r, s, and t with the respective radii r_q, r_r, r_s, and r_t, the face angle a at the center of the sphere type q is calculated from Equation A1.

$$\cos a = \frac{r_q(r_q + r_r + r_t) - r_r r_t}{(r_q + r_r)(r_q + r_t)} \tag{A1}$$

Face angles b and c are similarly obtained. The spherical angle α is calculated form a, b, and c.

$$\cos \alpha = \frac{\cos a - \cos b \cos c}{\sin b \sin c} \tag{A2}$$

The spherical angles β and γ are similarly obtained.

Then, the solid angle in fraction of sphere subtended at sphere q by the sphere r, s, and t is obtained from

$$A^q_{rst} = \frac{(\alpha + \beta + \gamma - \pi)}{4\pi} \tag{A3}$$

From the particle size and matrix green density, the relative number of type q sphere (x_q) is obtained. The frequency of appearance of type q spheres (k_q) is determined by $k_q = x_q / A_q$, where A_q is an average

solid angle subtended at the spheres of type q by all the spheres.

In a binary mixture of spheres of type m and i, the relative frequencies of the tetrahedra are given as follows.

$mmmm$	$mmmi$	$mmii$	$miii$	$iiii$
k_m^4	$4k_m^3k_i$	$6k_m^2k_i^2$	$4k_mk_i^3$	k_i^4

The pore volume in a tetrahedral subunit is obtained by subtracting particle volumes from the volume of a subunit. The volumes of a subunit (V) and a sphere (V_q) with the radius of r_q in the subunit are obtained from Equations A4 and A5.

$$9V^2 = 2r_qr_rr_sr_t(r_qr_r + r_qr_s + r_qr_t + r_rr_s + r_rr_t + r_sr_t) - (r_qr_rr_sr_t)^2\left(r_q^{-2} + r_r^{-2} + r_s^{-2} + r_t^{-2}\right) \quad \text{(A4)}$$

$$V_q = \frac{(\alpha + \beta + \gamma - \pi)}{3} r_q^3 \quad \text{(A5)}$$

References

1. M. N. RAHAMAN, "Ceramic Processing and Sintering" (Marcel Dekker, New York, 1995) p. 595.
2. C.-F. FAN and M. N. RAHAMAN, *J. Amer. Ceram. Soc.* **75** (1992) 2056.
3. L. C. DE JONGHE, M. N. RAHAMAN and C. H. HSUEH, *Acta Metall.* **34** (1986) 1467.
4. M. W. WEISER and L. C. DE JONGHE, *J. Amer. Ceram. Soc.* **71** (1988) C-125.
5. T. KIMURA, H. KAJIYAMA, R. YAZAKI and T. YAMAGUCHI, *J. Mater. Sci.* **31** (1996) 4149.
6. Y. NAKADA, M. ITOH and T. KIMURA, "Ceramic Processing Science (Ceramic Transactions, Vol. 83)" (American Ceramic Society, Westerville, OH, 1998) p. 541.
7. B. SERIER and D. TREHEUX, *Acta Metall. Mater.* **41** (1993) 369.
8. S. F. WANG, J. P. DOUGHERTY, W. HUEBNER and J. G. PEPIN, *J. Amer. Ceram. Soc.* **77** (1994) 3051.
9. K. MAEKAWA, Y. NAKADA and T. KIMURA, "Sintering Science and Technology" (The Pennsylvanis State University, State College, PA, 2000) p. 69.
10. D. TREHEUX, P. LOURDIN, B. MBONGO and D. JUVE, *Scripta Metall. Mater.* **31** (1994) 1055.
11. W. D. KINGERY and B. FRANCOIS, "Sintering and Related Phenomena" (Gordon and Breach, Science Publishers, New York, 1967) p. 471.
12. O. SUDRE and F. F. LANGE, *J. Amer. Ceram. Soc.* **75** (1992) 519.
13. Y. NAKADA and T. KIMURA, *ibid.* **80** (1997) 401.
14. O. SUDRE, G. BAO, B. FAN, F. F. LANGE and A. G. EVANS, *ibid.* **75** (1992) 525.
15. F. F. LANGE, *J. Mater. Res.* **2** (1987) 59.
16. R. M. GERMAN, "Particle Packing Characteristics" (Metal Powder Industries Federation, Princeton, New Jersey, 1989) p. 135.
17. P. LE GOFF, D. LECLERC and J. DODDS, *Powder Technology* **42** (1985) 47.
18. J. A. DODDS, *J. Colloid Interface Sci.* **77** (1980) 317.
19. M. W. WEISER and L. C. DE JONGHE, *J. Amer. Ceram. Soc.* **69** (1986) 822.
20. R. RAJ and R. K. BORDIA, *Acta Metall.* **32** (1984) 1003.
21. T. GARINO and H. K. BOWEN, *J. Amer. Ceram. Soc.* **73** (1990) 251.
22. Y. MASUDA and R. WATANABE, "Sintering Processes (Materials Science Research, Vol. 13)" (Plenum, New York, 1980) p. 3.
23. G. W. SCHERER, *J. Amer. Ceram. Soc.* **70** (1987) 719.

Received 21 March 2000
and accepted 28 August 2001